Water Supply

IWA PUBLISHING

Water Supply Vol 23 No 2, 738 doi: 10.2166/ws.2023.018

A novel integrated approach for monitoring drought stress in an aeolian desertification area using Vegetation Drought Status Index

Zhixin Zhao[a,b], Qi Liu[a,b], Aidi Huo[a,b,*], Yuxiang Cheng[c], Wenke Guan[d], EL-Sayed Abuarab Mohamed[e], Ali Mokhtar[e] and Ahmed Elbeltagi[f]

[a] School of Water and Environment, Chang'an University, Xi'an, Shaanxi 710054, China
[b] Key Laboratory of Subsurface Hydrology and Ecological Effects in Arid Region, Ministry of Education, Chang'an University, Xi'an, China
[c] College of Geology Engineering and Geomatics, Chang'an University, Xi'an, Shaanxi 710054, China
[d] Afforestation Desert Control Research Institute, Xinjiang Academy of Forestry, Urumqi 830000, China
[e] Faculty of Agriculture, Cairo University, Giza 12613, Egypt
[f] Agricultural Engineering Department, Faculty of Agriculture, Mansoura University, Mansoura 35516, Egypt
*Corresponding author. E-mail: huoaidi@chd.edu.cn

AH, 0000-0002-6216-5236

ABSTRACT

Drought is a costly natural disaster. The accuracy and applicability of different drought indexes in drought monitoring at different research areas are also different. Based on remote sensing (RS) and geographic information system technology, we propose a new RS-based drought index, Vegetation Drought Status Index (VDSI), for agricultural drought monitoring in both arid and humid regions using multi-sensor data. This index combines the Normalized Difference Vegetation Index (NDVI) data from Moderate Resolution Imaging Spectroradiometer (MODIS) sensor and data from 81 verification points regarding the *in situ* soil drought status. The model was applied to drought monitoring in Xinjiang Uygur Autonomous Region of China. Based on the comprehensive influence of water absorption on the reflectance spectrum of vegetation and soil, the reflectance of soil in MODIS bands B6 and B7 is generally higher than that of vegetation, so the model can directly obtain the surface soil moisture index. The correlation analysis ($R^2 > 0.79$) was valid; the change trends were the same; i.e., VDSI is a reliable referential index for agricultural drought monitoring.

Key words: drought monitoring, MODIS, RS, soil moisture, Xinjiang

HIGHLIGHTS

- A new drought index based on remote sensing – Vegetation Drought State Index (VDSI) was proposed.
- The model can directly obtain the surface soil moisture index.
- The results are applicable to agricultural drought monitoring in arid and humid regions.

1. INTRODUCTION

Drought is a universal natural phenomenon in the world, which has a wide range and a long duration. It is one of the most serious natural disasters affecting agricultural production and human life. The traditional drought monitoring method is based on limited data from meteorological observation stations. Although spatial interpolation can be carried out for the data, there are many uncertainties in drought monitoring due to the influence of many factors, such as sample size, spatial distribution characteristics and so on.

Remote sensing (RS) can quickly and accurately collect the related information of the surface features and has the characteristics of high time efficiency and wide monitoring range (Bowers & Hanks 1965; Tian *et al.* 2019; Huo *et al.* 2022a), which makes it become the research hotspot and frontier in the field of drought monitoring. In order to monitor drought quickly and widely, it is necessary to use satellite RS image data to monitor the surface of the observation area. The thermal inertia model was established using the diurnal range of surface temperature (Watson 1952). Rosema *et al.* (1992) improved upon this model for daily evapotranspiration and thermal inertia. Qi *et al.* (2003) combined plant cover information and land surface temperature to research Chinese drought using the Temperature Vegetable Drought Index.

In any drought monitoring technique, soil moisture is the key factor in agriculture domains, ecology, hydrology, and climate. Soil moisture is important in energy exchange and matter between the atmosphere and land surface. Because of the sparsity of sample points, the limited representative range, and the poor timeliness of data collection, especially in the macro and large-scale monitoring of soil moisture content, most of the conventional soil moisture measurement methods have the problem of replacing areas with points, and it is difficult to give the boundaries between different soil moisture content areas (Rhee *et al.* 2010; Luo *et al.* 2018a; Gorlé *et al.* 2019). In the RS monitoring of drought, because soil moisture is affected by many factors, such as temperature, rainfall, soil texture, and the interference of vegetation coverage cannot be ignored, the RS inversion of soil moisture has always been difficult.

Soil moisture can be rapidly depleted when precipitation is insufficient, so soil moisture can be used as the evaluation basis for areas suffering rain shortages. A variety of feasible and reliable methods to measure soil moisture currently exist from the point scale to the area scale (Huo *et al.* 2016a, 2020a; Luo *et al.* 2018b). Soil moisture is an important indicator of agricultural drought monitoring. Vegetation status and surface temperature can reflect water stress status. In the visible and near-infrared bands, the focus of RS drought monitoring is the change of vegetation index. The theoretical basis is the strong absorption and strong reflection characteristics of vegetation (crops, etc.) in these two bands (Huo *et al.* 2011a, 2020b).

There are many methods to monitor drought using RS technology. At present, thermal inertia model (Huo *et al.* 2016a), vegetation water supply index (Huo *et al.* 2011a), vegetation water shortage index (Huo *et al.* 2009), vegetation state index (Huo *et al.* 2010), vegetation index (Luo *et al.* 2019), and surface temperature are mainly used (Bayissa *et al.* 2019; Nguyen *et al.* 2019). Although RS has been applied to regional drought monitoring for a long time, the research of drought RS monitoring is mostly applied to the areas with single vegetation or flat terrain in the North of China, but less for the Northwest arid areas with diverse landforms, sparse vegetation, and less rainfall.

The primary focus of this research is a new drought monitoring methodology called the Vegetation Drought Status Index (VDSI), which satellite-based earth observations and integrates historical measurement data with soil, land use, and land cover. In order to monitor drought quickly and widely, it is necessary to monitor the surface of the observation area. Based on the spectral reflection characteristics of water, this study analyzes the common characteristics of water-bearing soil and vegetation and proposes the new VDSI suitable for the mixed region of soil and vegetation. It combines historical survey data with satellite-based earth observation data for drought monitoring in mixed areas, such as bare land and plants. This method combined with the new data mining analysis technology to identify the historical climate vegetation relationship related to the drought phenomenon.

2. STUDY AREA AND METHODOLOGY

2.1. Study area and data set

The study area, in Xinjiang Uygur Autonomous Region in China, is located between 73°40′–96°23′E and 34°25′–49°10′N at both sides of the Tarim River Basin and Gurbantunggut Desert in the Northwest of China, in the center of Eurasia, North–South width of 1,650 km, East–West length of 2,000 km, a total area of 1.66 million km^2, and borders eight countries including Russia, Kazakhstan, Tajikistan, Kyrgyzstan, Mongolia, Afghanistan, Pakistan, and India. Xinjiang is located in the center of Eurasia, far away from the ocean, surrounded by mountains, so the precipitation is rare. The annual average precipitation is only 150 mm in Xinjiang, and the spatial and temporal distribution is extremely uneven. Because of the surrounding high mountains and little precipitation, the average annual precipitation in the plain area is less than 100 mm. Due to the lack of precipitation and very little cloud cover in Xinjiang; the annual sunshine hours are extended. Generally, the temperature change is higher in the South than in the North, and the vertical decline is obvious in the mountains (Li 2021). Soil drought and land desertification have plagued the area in recent years. Figure 1 shows a sketch in the study area.

MODIS data have a wide range of bands and high time resolution, which has a great application value for real-time earth observation (Huo *et al.* 2011b, 2019). Therefore, MODIS data were selected as the main RS data source in this paper. MODIS data come from Warehouse Inventory Search Tool (WIST; http://Wist.echo.nasa.gov/api/). MOD11A2 is an 8 d synthesis data with a spatial resolution of 1 km × 1 km. MOD13A3 is a monthly vegetation index product including NDVI (Normalized Difference Vegetation Index), EVI (Enhanced Vegetation Index), blue light and other visible light, near-infrared, mid-infrared, thermal red light band reflectivity, and other auxiliary information.

2.2. Relationship between spectral reflectance and drought

Satellite RS images are reflections of surface features characterized by their thermal radiation and electromagnetic waves. Their electroreflectance and thermal radiation are different because of different structures and physicochemical properties

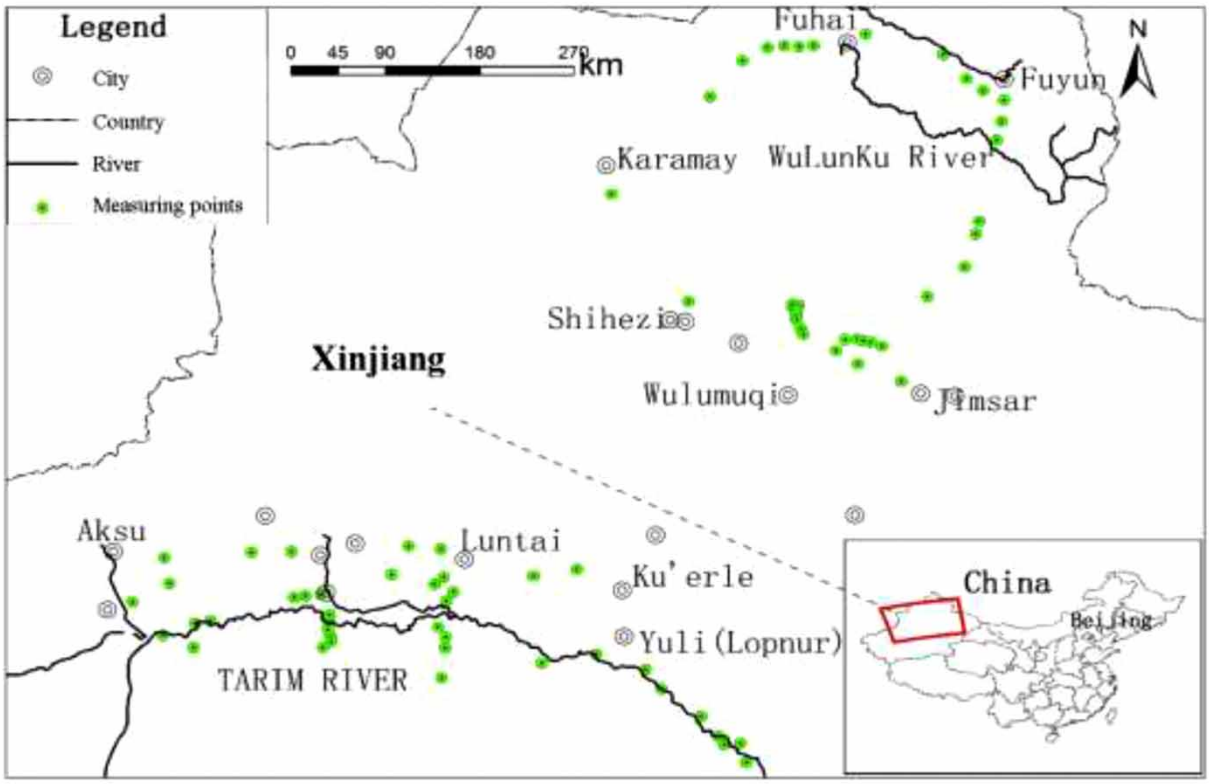

Figure 1 | The land synchronization measuring points distribution.

of surface features. Almost all incident energy, ranging across mid-infrared and near-infrared bands, is absorbed by water. Contrary, soil and plants absorb very little energy but reflect most of the energy in these ranges. Because of these different characteristics, the relationship between spectral reflectance and soil drought is clearly to be distinguished.

Figure 2 displays the absorption curve for water in wavelengths, where absorption peaks occur around 2.0 and 1.4 μm. Soil moisture is negatively correlated with reflectivity (The more soil moisture, the lower the reflectivity). The areas of low soil moisture are electromagnetic waves near 2.0 and 1.4 μm (Chen & Xiao 1994; de Nijs *et al.* 2019; Teng *et al.* 2019; Huo *et al.* 2022b). The sixth band wavelength is 1.628–1.652 μm, and the seventh band is 2.105–2.155 μm in MODIS data, which is near the absorption trough and peak of water. In this study, these two bands were used for soil drought inversion in MODIS image data.

2.3. Drought model

Soil is a complex containing many components. The soil spectrum is influenced by water, soil parent material, organic matter, and other elements; the effect of soil moisture is specifically important. In a word, reflectivity decreases with the increase of soil moisture.

The drought course is relevant to the water cycle as a whole including storage in rivers and lakes, vegetation water consumption, soil moisture, and precipitation. However, soil moisture is usually utilized to represent the status of a drought. It is the key factor among them.

MODIS image data include 36 bands. One MODIS image covers a large-scale area (i.e., covers 2,330 $km^2 \times 5{,}000\ km^2$). Again, the sixth and seventh bands correspond to the water absorption peak band. The sixth band (b_6) is more sensitive than the seventh band (b_7) both to bare-soil reflectance and plant, but both have similar radiation values. At the lowest atmospheric influence, the moisture in the soil is represented by b_6 and that in plants by b_7. The result can be limited within -1 to 1 with $b_6 + b_7$ as the denominator. This model is simple and easily applied, but the re-sampling result of 2 km b_6 and b_7 has a higher resolution on soil moisture inversion (Huo *et al.* 2011b; Bayissa *et al.* 2019), so the Drought Status Index (DSI) was

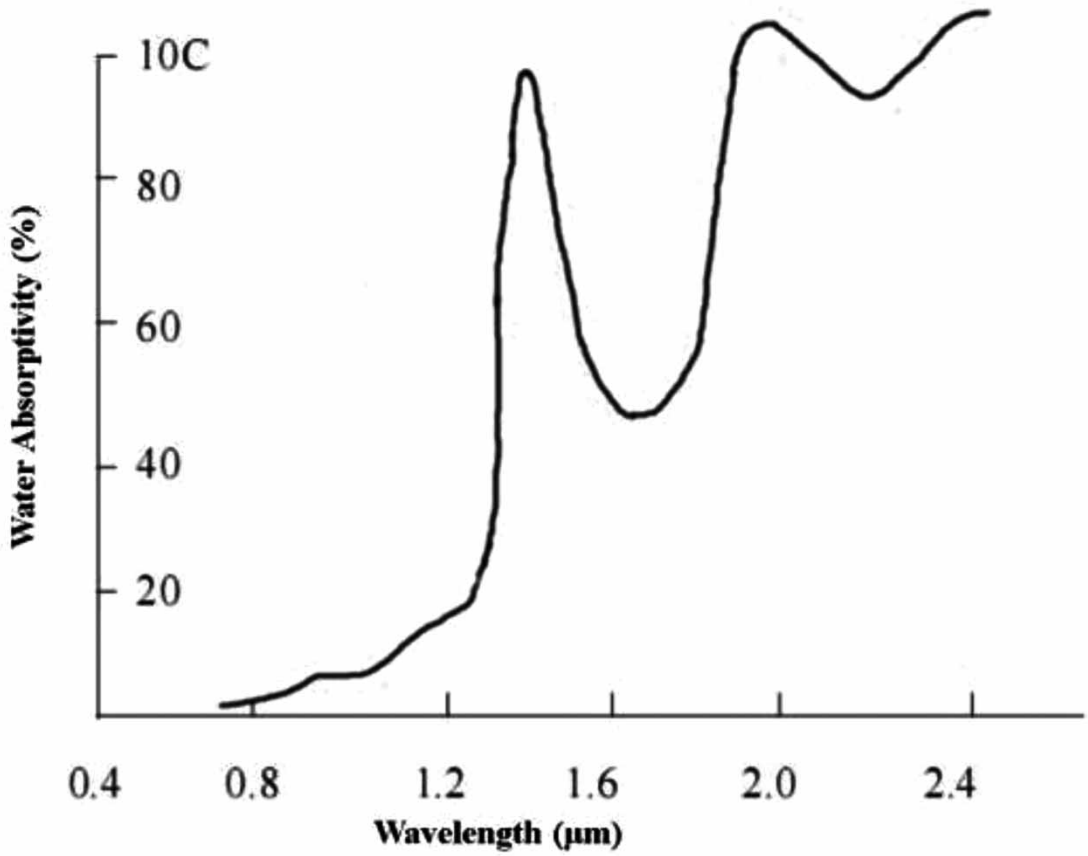

Figure 2 | The water absorption curve (Chen & Xiao 1994).

proposed and refined, and the model equation was as follows in Equation (1) (Huo *et al.* 2018):

$$\mathrm{DSI} = \frac{b'_6 - b'_7}{b'_6 + b'_7} \tag{1}$$

where $b'_6$and b'_7 are the re-sampling results of the b_6, b_7 bands in MODIS at 2 km scale. To improve the model and obtain more accurate monitoring results, a vegetation parameter f_v was added to calibrate the reflectance difference (b'_6 and b'_7 bands) for vegetation and bare soil. In most areas of Xinjiang, vegetation reflectance and bare land are obviously prominent, and the former reflectance is higher than the latter one. Because the reflectance of soil is higher than vegetation in b'_6 and b'_7 re-sampling bands, for index uniformity, droughts occurring over vegetation and bare-soil surfaces can be expressed in the following equations:

$$\mathrm{DSI_V} = f_v \times \mathrm{DSI} \tag{2}$$

$$\mathrm{DSI_S} = (1 - f_v) \times \mathrm{DSI} \tag{3}$$

where $\mathrm{DSI_V}$ and $\mathrm{DSI_S}$ are the drought indexes of vegetation and bare soil, respectively; f_v is the proportion of vegetation area per unit area The relationship expression of NDVI and f_v can be as follows in Equations (4) and (5) (Gutman & Ignatov 1998):

$$\mathrm{NDVI} = (b'_2 - b'_1)/(b'_2 + b'_1) \tag{4}$$

$$f_v = \frac{\mathrm{NDVI} - \mathrm{NDVI_{min}}}{\mathrm{NDVI_{max}} - \mathrm{NDVI_{min}}} \tag{5}$$

where b'_1 and b'_2 are the re-sampling results of the b_1, b_2 bands in MODIS at 2 km scale. Over the same period for a multi-year period, $NDVI_{max}$, $NDVI_{min}$ are the maximum and minimum NDVI values for the whole growing season ($NDVI_{max} = 0.82$; $NDVI_{min} = 0.01$ in this paper). In Xinjiang, there is more bare land present than land with sparse vegetation, so Equation (1), VDSI, can be rewritten as follows in Equation (6):

$$VDSI = \left[1 - 0.82 \times \frac{b'_2 - b'_1}{b'_2 + b'_1}\right] \times \frac{b'_6 - b'_7}{b'_6 + b'_7} \tag{6}$$

Based on the MODIS 1B data set, the relationship between the retrieval values from the RS image data sets and the field-work measure values of soil moisture were analyzed at six spatial scales from 1 km × 1 km to 32 km × 32 km, respectively. Huo *et al.* (2016b) indicate that 2 km scale is the suitable scale for the retrieval of soil moisture in the study area; 1 and 4 km are the second best scale. Compared with references (Huo *et al.* 2018), this paper used the newly resampled 2 km spatial resolution MODIS band B2 and band B1 to calculate the vegetation index and which can obtain more accurate calculation results. Therefore, it can be said that this paper introduces the revised vegetation index, develops the calculation formula in the reference (Huo *et al.* 2018), and makes the calculation results more accurate.

2.4. Application and verification of VDSI

The reason for Xinjiang's arid environment is that it is far away from the sea and surrounded by mountains. The water from the ocean gradually decreases in the long-distance transportation process and is blocked by mountains when it arrives at Xinjiang, which not only reduces the water content but also forms the regional difference in precipitation distribution.

There are two kinds of drought in Xinjiang caused by natural factors and human factors. Natural factors refer to the fact that Xinjiang is located in the Northwest inland of China, far away from the ocean and hard to reach by water vapor. In the North, West and South of Xinjiang, there are tall mountains to block the water from outside. In addition, the climate of Xinjiang belongs to the temperate continental climate, which is characterized by little precipitation and high temperature in summer. Human factors mainly refer to the destruction of forest vegetation here. Since the western development of Xinjiang, the population has increased rapidly, and the expansion of the city has destroyed a large number of vegetation. In addition, due to the increase of population and the increase of domestic and industrial water, the surface water and groundwater are overdrawn, which directly leads to the drought in Xinjiang.

The data source selected one MODIS image data from 2007. Spatial resolution is 1 km. The distribution of drought was analyzed by using the homochronous soil moisture data collected in the field in the study area; fieldwork is a significant part of model verification.

MODIS is the vital spectroradiometer on Terra. Its data are shared directly to the world. MODIS has three scales of resolution: 1,000, 500, and 250 m. The scanning width is 2,330 km. The satellite's transit times are 00:30 and 12:30 (Beijing time) in the study area. MODIS images at 12:30 were used to minimize the influence of cloud cover. The MODIS 1B data set was downloaded from WIST with 1 km resolution as a 16-bit attribute dataset (Luo *et al.* 2018a, 2018b; Sundell *et al.* 2019).

The surface observation time corresponds to the time when MODIS data were taken over. The observation site is in the area with desertified land distributed on both sides of Tarim River and the edge of Gurbantonggut desert in Xinjiang. The location of 81 measured data detected in July 2007 is shown in Figure 1. The data collection method was as follows: Firstly, we selected the area with a uniform surface cover distribution, with an area of about 1 km. Then we measured the longitude and latitude coordinates of the center points of each pixel near the area from the MODIS image and used GPS navigation to find the center point nearest to the center point of the actual measurement area, so that the measured area was completely arranged in a single pixel as far as possible. Lastly, from the middle point of the survey area, 100 m sample lines were arranged in four directions (South, East, North, and West), respectively, and the soil moisture content was measured at an interval of 20 m in each direction. The mean value of 21 sample points (including the center point, corresponding to the pixel location) was used to represent the actual soil moisture content of the surface. The soil moisture was calculated by the method of weighing and drying, that is, under the constant temperature of 100–105°C, bake to the dry state, and calculate the moisture content of the excavated sample by the weight before and after drying. Because the surface humidity retrieved by satellite is the comprehensive humidity of various surface features, the average humidity was used to represent the actual humidity within the observation range. The method and position of the observatory we used are similar to those used by Huo *et al.* (2009).

3. RESULTS AND ANALYSIS

3.1. RS monitoring drought results

Based on Equation (6), b_6', b_7', B_1 and B_2 data from the MODIS image data had been used to calculate the drought index distribution as shown in Figure 3.

A visual examination of Figure 3 shows that the intensity of drought depicted and general spatial patterns similar. In Xinjiang Uygur Autonomous Region of China, the VDSI-based drought status is in accordance with actual measurements, namely, the most severe drought area was Gurbantunggut Desert areas and the central portion of the Taklimakan. Especially in the most arid areas of Xinjiang, the improved 2 km spatial resolution image of VDSI is readily apparent, showing considerably higher detail at a local scale area. In a word, drought status can be divided into two parts: the drought in the North is mainly concentrated in the Gurbantunggut Desert, and the drought in the South is mainly concentrated in the Tarim River Basin. In the Southern part, the drought is serious in the center and light in the surrounding area, and many villages and towns are distributed in the light area. The main reason is strong sunshine and less precipitation. The Tarim River Basin is a severely arid region, although it is fed by inland rivers. This is mainly because water supply cannot fully meet ecological water demand. Most of the remaining areas are moderate, and the area of the non-drought region is very small.

The Takilimakan Desert is approximately 400 km in width in the South–Northwest direction and approximately 1,000 km in length in the East–West direction; it is located at the center of the Tarim Basin and it is the tenth largest desert in the world. Its total area is 330,000 km^2. The Gurbantunggut Desert is the second biggest desert in China. It is located at the center of the Junggar Basin with an area of about 48,800 km^2. The lowest soil moisture areas, shaded areas in Figure 3, are these two deserts across the study area. There are several cities, including Karamay, Shihezi, and Aksu, scattered throughout these areas which have higher soil moisture (light areas in Figure 3).

Table 1 shows the correlation between the soil moisture data from measurements and the VDSI by means of the Pearson correlation coefficient.

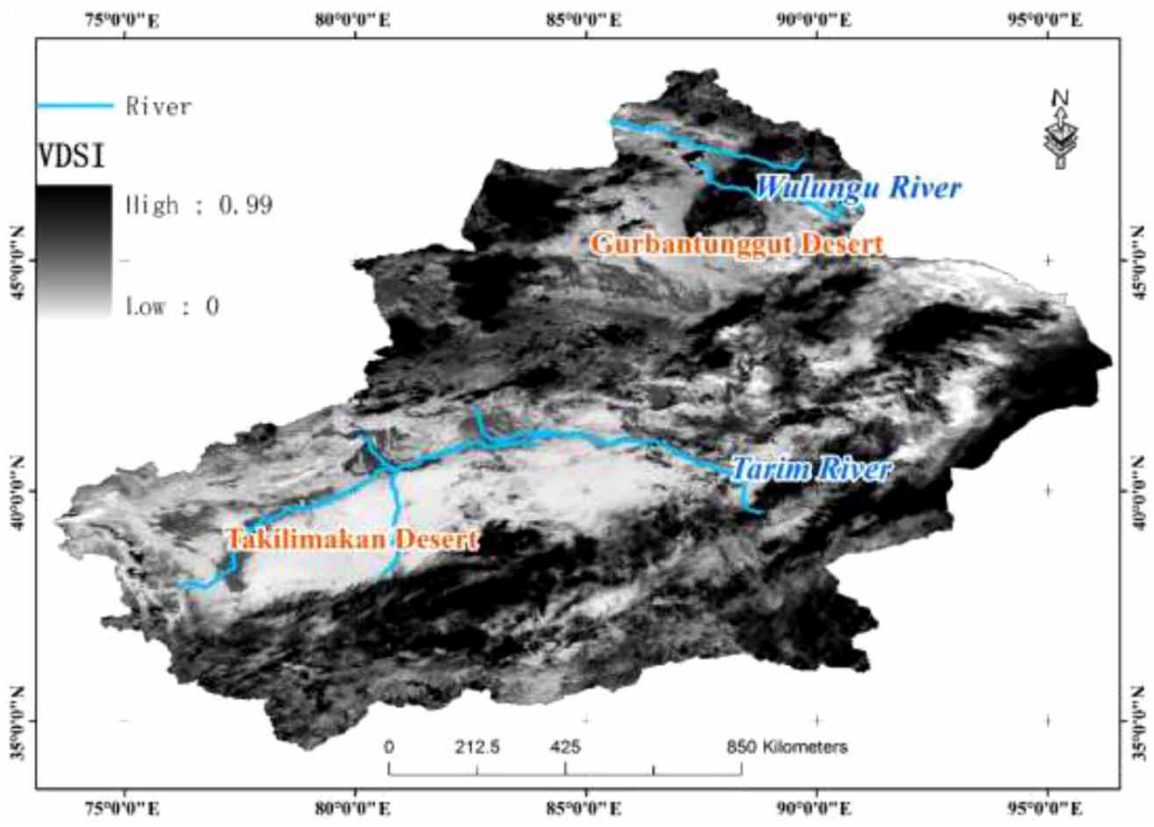

Figure 3 | The VDSI of Xinjiang Uygur Autonomous Region.

Table 1 | Correlation between soil moisture and VDSI using Pearson coefficient

Name	Parameters	VDSI	Soil moisture
VDSI	Pearson R	1	0.793
	Significant probability		0.001
	The number of sample points	81	81
Soil moisture	Pearson R	0.793	1
	Significant probability	0.001	
	The number of sample points	81	81

Confidence coefficient shown in Table 1 is higher than 0.79, indicating that the VDSI is accurate. The soil moisture model was refined as follows in Equation (7):

$$M(\%) = (0.98 \times \text{VDSI} - 0.44) \times 100 \tag{7}$$

where M is modified soil moisture. The Confidence Coefficient of the fitting result (R^2) was 0.79 and the average fitting error was 3.74%, so Equation (7) can also be used for the corrected calculation of soil moisture at a large-scale drought monitoring area.

VDSI model analyzes the reflection spectrum curve of water and comprehensively considers the influence of the absorption characteristics of vegetation and soil water on the spectrum reflection, with few input parameters and fast calculation, which is suitable for the needs of large-scale RS drought monitoring. Compared with NDVI and other index models, VDSI has little impact on soil vegetation coverage and reflects the comprehensive surface water content in a unified and intuitive way, which is very suitable for large data and large-scale drought monitoring research. Figure 4 is a scattered diagram between VDSI and soil moisture comprised of 81 points detected in July 2007.

Figure 4 shows the scattered diagram between measured soil moisture and VDSI. According to Figure 4, the data points can be divided into three areas: the first area is between 0 and 10%, and the distribution area is mainly desert; the second area is between 10 and 15%, and the distribution area is mainly on both sides of the Tarim River mainstream; the third area is between 15 and 30%, and the distribution area is mainly residential or water areas. Figure 4 shows that the VDSI

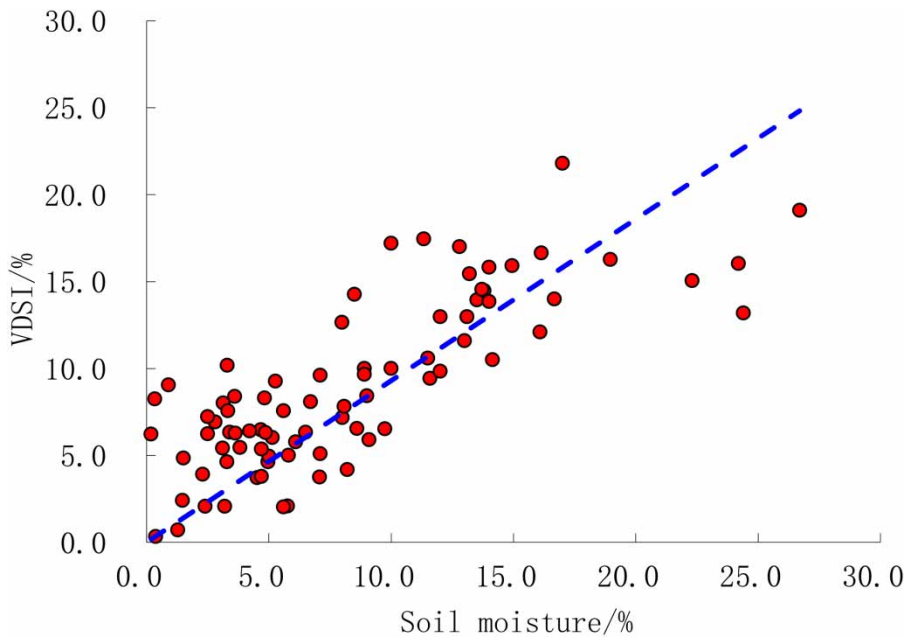

Figure 4 | A scatter diagram between VDSI and measured soil moisture.

value is slightly higher than the measured value, probably because the RS monitoring depth is relatively shallow (about 10 cm below the ground), while the actual measurement is generally about 20 cm below the ground surface, so the VDSI value is slightly higher than the measured value.

3.2. VDSI grade standards

The grade standards of VDSI were established based on Xinjiang's Statistical yearbooks, agricultural statistical yearbooks, drought statistical data, fieldwork data, and RS image data, as is shown in Table 2.

By the cluster analysis, the degree of drought is divided into five classes (Table 2), which are: (1) Particularly Severe Drought ($0 < \text{VDSI} \leq 0.028$) mainly distributed in desert areas, such as in Takilimakan Desert; (2) Severe Drought ($0.028 < \text{VDSI} \leq 0.083$) mainly distributed in sandy regions, such as in the Gurbantunggut Desert; (3) Moderate Drought ($0.083 < \text{VDSI} \leq 0.140$) mainly distributed in the Tarim River Basin; (4) Mild Drought ($0.140 < \text{VDSI} \leq 0.273$) and Normal ($0.273 < \text{VDSI} \leq 0.870$) mainly distributed in inhabited areas. The grading results for the study area were shown in Figure 5.

Table 2 | Grading index of drought monitoring by RS

Drought status	VDSI range
Particularly severe drought	$0<\text{VDSI} \leq 0.028$
Severe drought	$0.028<\text{VDSI} \leq 0.083$
Moderate drought	$0.083<\text{VDSI} \leq 0.140$
Mild drought	$0.140<\text{VDSI} \leq 0.273$
Normal	$0.273<\text{VDSI} \leq 0.870$

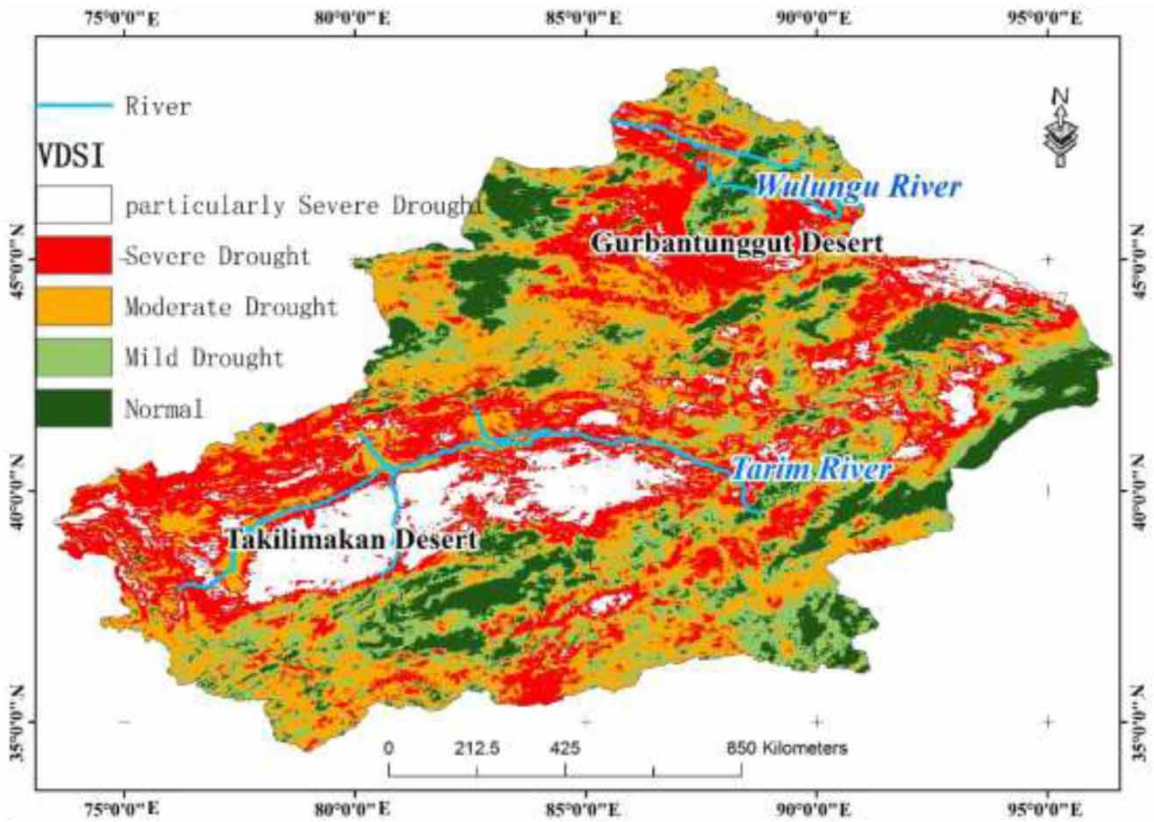

Figure 5 | The drought magnitude from RS monitoring in Xinjiang Province.

Figure 5 depicts the spatial distribution of drought in Xinjiang. Figure 5 map has classified particularly severe, severe, moderate, mild, and normal drought conditions for the same location depicted in Figure 3. As discussed earlier, Figure 3 is generated by the VDSI indicator to determine the overall level of drought status for a value. On the contrary, Figure 5 represents a single aspect of drought stress on five grade standards. Figure 5 classifies North-central Xinjiang as being in severe drought grades (indicated by the red color label in Figure 5) and classifies South-central Xinjiang as being in particularly severe drought (indicated by the white color label). This intuitively reflects that the drought level of the Taklimakan Desert is one level higher than that of Gurbantunggut Desert. Particularly, severe drought occurred on the South side of the Tarim River where the Takilimakan Desert hinterland is located; this area is approximately 19.6 km^2. The Eastern part of Xinjiang also has some particularly severe drought areas. The severe drought-grade region was located at the North side of the Gurbantunggut Desert and the Tarim River. This area was around 47 km^2; the moderate drought-grade region was distributed at the Southern, central, and Eastern edges of Xinjiang. It was about 48.4 km^2; the normal and mild drought regions were mainly located around larger cities with areas of 21.2 and 29.7 km^2, respectively.

4. DISCUSSION

The drought index is used to monitor, identify, and classify drought conditions. They allow for quantitative evaluation of the spatial extent, duration, and intensity of anomalous climatic conditions. Further analysis of satellite RS images in different months of the year shows that among the three different types of sandy land (fixed sandy, semi-fixed, and mobile land), the fixed sand land has the largest change in soil moisture content, and the mobile sand land has the smallest change in soil moisture. The mobile sandy land has the largest soil moisture, followed by the semi-fixed sandy land and the fixed sandy land. The climatic conditions change periodically with seasons, and the water content of sandy land also changes with time (Feng *et al.* 2001; Du *et al.* 2007; Tracy & Corcoran 2014; Sposito *et al.* 2019). In May, September, and October, the soil moisture of the sandy land is relatively high, which is related to the fact that the rainfall in this area is mainly concentrated over spring and autumn, which further indicates that rainfall is the main supply mode of soil moisture in sandy land. In July and August, the water content of sandy land is relatively low, which is due to the small rainfall, high temperature, and large evaporation, resulting in a large loss of soil water, but not timely and effective recharge. Therefore, when afforestation is carried out in the arid and desertification areas, the spring and autumn periods with high soil moisture content should be selected.

Due to the high temporal resolution of MODIS image data, but the low spatial resolution, the following aspects should be considered to further improve the accuracy and quality in RS drought monitoring: the fusion technology of multi-source RS data should be considered in the follow-up research work; the ground survey is the measured soil moisture within 1–20 cm of the ground, and the RS inversion depth is the moisture content within 10 cm under the ground surface. The relationship between the two different depths needs further accurate calculation; as the transit time of the satellite in the sky above the study area is only a few minutes, and the actual measurement time on the ground is generally between 9:00 and 16:00, the time out of sync will also cause errors, so the later field investigation should try to keep the same time with the transit time of the satellite in the sky. Further studies are necessary to develop the VDSI to enhance its applicability to different seasons, scales, and regions.

Differences among statistical methods and cloud cover in various agricultural departments caused some errors between statistical data and VDSI results in regard to some specific drought areas. Overall, VDSI still presented reliable reference data for the droughts status across Xinjiang. In future research, the change in surface temperature and the influence of different resolution scales on the inversion results will be studied with regard to the development of the model.

The outcomes of this study suggest, in line with the most recent applications of remote soil moisture, that VDSI has good potential in monitoring drought, especially in the arid and desertification areas. With the forthcoming availability of microwave, optical, and thermal data streams, this study supports the development of innovative trails for enhanced drought monitoring.

5. CONCLUSIONS

A new drought indicator was presented based on the inverse of the MODIS image data, which in turn is related to the soil moisture content. The Xinjiang case study results indicated that VDSI actually reflects the drought status. Our primary conclusions can be summarized as follows.

(1) A new RS monitoring model of VDSI which is appropriate for Xinjiang Uygur Autonomous Region of China was proposed by using the composite information of multiple bands of MODIS satellite image data and considering the spectral reflection characteristics of water. It is of great importance to the operational process of drought monitoring.
(2) The VDSI RS monitoring model can precisely reflect the spatial change characteristics of drought in the study area. The VDSI model was utilized to monitor the drought state on both sides of Tarim River and the edge of Gurbantonggut desert. Through the correlation analysis and verification with the VDSI value and *in situ* soil moisture obtained at the same time, Confidence Coefficient was higher than 0.79. The linear correlation was significant.
(3) The drought area of each drought class is mainly consistent with the fluctuation trend of statistical data. The comparison between the drought area obtained by RS monitoring and the drought area obtained by field survey shows that VDSI is a responsible reference for agricultural drought application.

ACKNOWLEDGEMENTS

The authors appreciate Dr Xiangwu Kang from the Institute of Scientific and Technical Information of China for valuable comments and suggestions for this paper, and Dr Duanyang Xu and Ming Hou for providing the field survey data. We would also like to give thanks to Eric Holt from the UNL Writing Center for correcting the English expressions. The authors thank all anonymous reviewers and the editor for their constructive comments, which significantly improved the quality of this article.

FUNDING

This work was supported by the National Natural Science Foundation of China (Grant No. 42261144749); National Natural Science Foundation of China (Grant Nos. 41877232, 41672255, and 41790444); National Key R&D Program of China (2018YFE0103800); the Fundamental Research Funds for the Central Universities, CHD (300102299302); Key Laboratory Open Project Fund of State Key Laboratory of Loess and Quaternary Geology, Institute of Earth Environment, CAS (Grant No. SKLLQG1909).

DATA AVAILABILITY STATEMENT

All relevant data are included in the paper or its Supplementary Information.

CONFLICT OF INTEREST

The authors declare there is no conflict.

REFERENCES

Bayissa, Y., Tadesse, T. & Demisse, G. 2019 Building a high-resolution vegetation outlook model to monitor agricultural drought for the Upper Blue Nile Basin, Ethiopia. *Remote Sensing* **11** (4), 371.

Bowers, S. & Hanks, R. 1965 Reflection of radiant energy from soils. *Soil Science* **100** (2), 130–138.

Chen, W. & Xiao, Q. 1994 Application of drought monitoring with anomaly vegetation index in 1992. *Environmental Remote Sensing* **9** (2), 106–112. (in Chinese, with English abstract).

De Nijs, E. A., Hicks, L. C., Leizeaga, A., Tietema, A. & Rousk, J. 2019 Soil microbial moisture dependences and responses to drying–rewetting: the legacy of 18 years drought. *Global Change Biology* **25** (3), 1005–1015.

Du, X., Wang, S., Zhou, Y. & Wei, H. 2007 Construction and validation of a new model for unified surface water capacity based on MODIS data. *Geomatics and Information Science of Wuhan University* **32** (3), 205–207.

Feng, Q., Cheng, G. & Endo, K. 2001 Water content variations and respective ecosystems of sandy land in China. *Environmental Geology* **40** (9), 1075–1083.

Gorlé, C., Zeoli, S., Emory, M., Larsson, J. & Iaccarino, G. 2019 Epistemic uncertainty quantification for Reynolds-averaged Navier–Stokes modeling of separated flows over streamlined surfaces. *Physics of Fluids* **31** (3), 035101.

Gutman, G. & Ignatov, A. 1998 The derivation of the green vegetation fraction from NOAA/AVHRR data for use in numerical weather prediction models. *International Journal of Remote Sensing* **19** (8), 1533–1543.

Huo, A., Kang, X., Liu, Z.-l. & Cao, X.-s. 2009 Simplified split-window algorithm model to retrieve land surface temperature in aeolian desertification area with MODIS image data – taking North Shaanxi Province as an example. *Journal of Earth Sciences and Environment* **3**, 016. (in Chinese, with English abstract).

Huo, A., Kang, X., Zhang, G. & Wu, S. 2010 Study on soil moisture model in Mu Us desertification using MODIS image. *Agricultural Research in the Arid Areas S* **28** (4), 19–23. (in Chinese, with English abstract).

Huo, A., Chen, X., Li, H., Ming, H. & Hou, X. 2011a Development and testing of a remote sensing-based model for estimating groundwater levels in aeolian desert areas of China. *Canadian Journal of Soil Science* **91** (1), 29–37.

Huo, A., Xie, J., Sun Z. & Zhou, L. 2011b Methodology of land surface broadband albedo retrieval in the desertification area based on MODIS image data. International Symposium on Water Resource and Environmental Protection, Xi'an, China, 2011, pp. 2539–2542.

Huo, A., Dang, J., Song, J. X., Chen, X. H. & Mao, H. R. 2016a Simulation modeling for water governance in basins based on surface water and groundwater. *Agricultural Water Management* **174**, 22–29.

Huo, A., Zhang, J., Cheng, Y., Yi, X., Qiao, L., Su, F., Du, Y. & Mao, H. 2016b Assessing the effect of scaling methods on retrieval of soil moisture based on MODIS images in arid regions. *Toxicological and Environmental Chemistry* **98**, 3–4.

Huo, A., Wei, H., Cheng, Y.-x., Zheng, C.-l., Guan, W.-k., Song, J.-x. & Qiao, L. 2018 Novel drought monitoring model based on MODIS image data. *Acta Scientific Agriculture* **2** (10), 93–99. doi: 10.31080/ASAG.2018.02.0201.

Huo, A., Wang, X., Liang, Y., Jiang, C. & Zheng, X. 2019 Integrated numerical model for irrigated area water resources management. *Journal of Water and Climate Change*. https://doi.org/102166/wcc2019042

Huo, A., Yang, L., Peng, J., Cheng, Y. & Jiang, C. 2020a Spatial characteristics of the rainfall induced landslides in the Chinese Loess Plateau. *Human and Ecological Risk Assessment: An International Journal* **26** (9), 2462–2477. doi: 10.1080/10807039.2020.1728517.

Huo, A., Huang, Z., Cheng, Y. & Van Liew, M. W. 2020b Comparison of two different approaches for sensitivity analysis in Heihe river basin (China). *Water Supply* **20** (1), 319–327.

Huo, A., Wang, X., Zhao, Z., Yang, L., Zhong, F., Zheng, C. & Gao, N. 2022a Risk assessment of heavy metal pollution in farmland soils at the northern foot of the Qinling Mountains, China. *International Journal of Environmental Research and Public Health* **19**, 14962. doi:10.3390/ijerph192214962.

Huo, A., Zhao, Z., Luo, P., Zheng, C., Peng, J. & Abuarab, M. E.-S. 2022b Assessment of spatial heterogeneity of soil moisture in the critical zone of gully consolidation and highland protection. *Water* **14**, 3674.

Li, Y. N. 2021 *Research on the Temporal and Spatial Characteristics of Xinjiang NDVI From 2001 to 2020 and its Response to Environmental Factors*. Xinjiang University. doi:10.27429/d.cnki.gxjdu.2021.001240.

Luo, P., He, B., Duan, W., Takara, K. & Nover, D. 2018a Impact assessment of rainfall scenarios and land-use change on hydrologic response using synthetic area IDF curves. *Journal of Flood Risk Management* **11**, S84–S97.

Luo, P., Zhou, M., Deng, H., Lyu, J., Cao, W., Takara, K., Nover, D. & Schladow, S. G. 2018b Impact of forest maintenance on water shortages: hydrologic modeling and effects of climate change. *Science of The Total Environment* **615**, 1355–1363.

Luo, P., Kang, S., Apip, Zhou, M., Lyu, J., Aisyah, S., Binaya, M., Regmi, R. K. & Nover, D. 2019 Water quality trend assessment in Jakarta: a rapidly growing Asian megacity. *PLOS ONE* **14** (7), e0219009. https://doi.org/10.1371/journal.pone.0219009.

Nguyen, H., Wheeler, M. C., Otkin, J. A., Frost, A. J., Stone, R. C. & Cowan, T. 2019 Using evaporative stress index to monitor flash drought in Australia. *Environmental Research Letters* **14** (6), 064016.

Qi, S., Wang, C. & Niu, Z. 2003 A national drought monitoring study using temperature vegetation drought index (TVDI). *Journal of Remote Sensing* **7** (5), 420–427. (in Chinese, with English abstract).

Rhee, J., Im, J. & Carbone, G. J. 2010 Monitoring agricultural drought for arid and humid regions using multi-sensor remote sensing data. *Remote Sensing of Environment* **114** (12), 2875–2887.

Rosema, A., Verhoef, W., Noorbergen, H. & Borgesius, J. 1992 A new forest light interaction model in support of forest monitoring. *Remote Sensing of Environment* **42** (1), 23–41.

Sposito, J. C. V., Francisco, L. F. V., Crispim, B. D. A., Dantas, F. G. D. S., Souza, J. P. D., Viana, L. F., Solórzano, J. C. J., Oliveira, K. M. P. D. & Barufatti, A. 2019 Influence of land use and cover on toxicogenetic potential of surface water from Central-West Brazilian Rivers. *Archives of Environmental Contamination and Toxicology* **76** (3), 483–495.

Sundell, J., Haaf, E., Norberg, T., Alen, C., Karlsson, M. & Rosen, L. 2019 Risk mapping of groundwater-drawdown-induced land subsidence in heterogeneous soils on large areas. *Risk Analysis* **39** (1), 105–124.

Teng, H., Branstator, G., Tawfik, A. B. & Callaghan, P. 2019 Circumglobal response to prescribed soil moisture over North America. *Journal of Climate* **32** (14), 4525–4546.

Tian, J., Song, S. & He, H. 2019 The relationship between soil emissivity and soil reflectance under the effects of soil water content. *Physics and Chemistry of the Earth, Parts A/B/C* **110**, 133–137.

Tracy, F. T. & Corcoran, M. K. 2014 Effect of changes in hydraulic conductivity on exit gradient at selected levee systems using numerical models. *Open Hydrology Journal* **8** (1), 27–40.

Watson, K. M. 1952 The effect of final state interactions on reaction cross sections. *Physical Review* **88** (5), 1163.

First received 28 September 2022; accepted in revised form 17 January 2023. Available online 30 January 2023